

sition from a localized solvent-bound ground state to the continuum of the solvent conduction band (22), the absorption of electrons in contact pairs should be similar to the absorption of the free  $e_s^-$ . Although the spectra are similar, the stark contrast between the difference signals for the three-pulse experiments shown in the insets of Figs. 2B and 3B verifies that indeed two different species are absorbing the 2000-nm pulse of light. Because recombination is initially promoted when the electron is excited at long times and hindered for excitation at short times, we argue that two different species account for  $e_s^-$  in the immediate and solvent-separated contact pairs.

The ET reaction being controlled in this case, the recombination of the CTTS electron with  $Na^0$  to reform  $Na^-$ , starts from one of two well-defined configurations, an immediate or solvent-separated contact pair. Both configurations undergo a spontaneous ET reaction when the electron excitation pulse is applied to alter the reaction dynamics. When the electron excitation pulse arrives at early times, the excess energy delocalizes the electrons in the immediate contact pairs, distributing them out into the solvent in much the same manner as if a single excitation pulse had been used with the same total energy. The effect of the excitation pulse in shutting off the recombination of immediate contact pairs is rate-limited by the translational motions of the solvent required to eject the electron from the immediate cavity. If the electron excitation pulse comes at later times when no immediate contact pairs are present, the delocalized electron has some probability to transfer back onto the nearby  $Na^0$  (once the solvent has rearranged), creating a hot  $Na^-$  that cools on the  $\sim 2$ -ps time scale. Some of the electrons in solvent-separated contact pairs that absorb the 2000-nm pulse can move in directions away from the sodium atom, resulting in a cessation of recombination at longer times.

All of these results demonstrate that it is possible to use femtosecond pulse sequences to control both the position of the electron and the rate of recombination in CTTS reactions. These CTTS systems have only electronic degrees of freedom, so we can control ET reactions without having to precisely shape the femtosecond pulses, as would be necessary to control the nuclear degrees of freedom in photodissociation reactions (23). For the  $Na^-$  CTTS reaction, the wavelength of the excitation pulse can be chosen to create a desired initial ratio of immediate to solvent-separated contact pairs. Subsequent excitation at 2000 nm can then be used to selectively break up the immediate pairs or to manipulate the recombination dynamics of solvent-separated pairs. The use of electron excitation pulses at different wavelengths or with different relative polarizations may offer an even finer degree of control, possibly allowing further enhancement of the recombination of

solvent-separated pairs. Perhaps most importantly, the use of multiple femtosecond pulses provides a window on the solvent motions that drive ET reactions.

References and Notes

1. R. A. Marcus, N. Sutin, *Biochim. Phys. Acta* **811**, 265 (1985).
2. P. F. Barbara, T. J. Meyer, M. A. Ratner, *J. Phys. Chem.* **100**, 13148 (1996).
3. M. J. Blandamer, M. F. Fox, *Chem. Rev.* **70**, 59 (1970).
4. W.-S. Sheu, P. J. Rossky, *J. Phys. Chem.* **100**, 1295 (1996).
5. E. R. Barthel, I. B. Martini, B. J. Schwartz, *J. Chem. Phys.* **112**, 9433 (2000).
6. I. B. Martini, E. R. Barthel, B. J. Schwartz, *J. Chem. Phys.* **113**, 11245 (2000).
7. E. R. Barthel, I. B. Martini, B. J. Schwartz, *J. Phys. Chem.* in press.
8. V. H. Vilchiz, J. A. Kloepper, A. C. Germaine, V. A. Lenchenkov, S. E. Bradforth, *J. Phys. Chem. A* **105**, 1711 (2001).
9. J. L. Dye, *Prog. Inorg. Chem.* **32**, 327 (1984).
10. W. A. Seddon, J. W. Fletcher, *J. Phys. Chem.* **84**, 1104 (1980).
11. L. M. Dorfman, F. Y. Jou, R. Wageman, *Ber. Bunsenges. Phys. Chem.* **75**, 681 (1971).
12. B. Bockrath, L. M. Dorfman, *J. Phys. Chem.* **79**, 1509 (1975).
13. P. Piotrowicz, J. R. Miller, *J. Am. Chem. Soc.* **113**, 5086 (1991).
14. Z. Wang, O. Shoshana, S. Ruhman, in *Proceedings of the 12<sup>th</sup> International Conference on Ultrafast Phenomena*, vol. 66 of *Springer Series in Chemical Physics* (Springer-Verlag, Berlin, 2001), pp. 624–626.

15. Z. Wang, O. Shoshana, S. Ruhman, in preparation.
16. M. P. Debreczeny, W. A. Svec, E. M. Marsh, M. R. Wasielewski, *J. Am. Chem. Soc.* **118**, 8174 (1996).
17. T. W. Kee, D. H. Son, P. Kambhampati, P. F. Barbara, *J. Phys. Chem.*, in press.
18. D. H. Son, P. Kambhampati, T. W. Kee, P. F. Barbara, *J. Am. Chem. Soc.*, in press.
19. M. T. Lok, F. J. Tehan, J. L. Dye, *J. Phys. Chem.* **76**, 2975 (1972).
20. It is also possible that the 2000-nm pulse promotes the electron into the excited CTTS state,  $Na^{*-}$ , and that this state absorbs 490-nm light. The 700-fs rise of the difference signal would then represent the time for internal conversion to form  $Na^-$  from  $Na^{*-}$ . In (5), we determined the spectrum of  $Na^{*-}$  and found no oscillator strength at 490 nm. However, we expect the position of the spectrum to be very sensitive to the local solvent configuration around the  $Na^{*-}$ , and the solvent configuration around  $Na^{*-}$  produced directly from the ground state is quite different from that produced by reexcitation of the electron in a contact pair. Further experiments with different probe wavelengths should clarify this issue.
21. L. Reynolds, J. A. Gardecki, S. J. V. Frankland, M. L. Horng, M. Maroncelli, *J. Phys. Chem.* **100**, 10337 (1996).
22. See, e.g., H. T. Davis, R. G. Brown, *Adv. Chem. Phys.* **31**, 329 (1975).
23. See, e.g., A. Assion *et al.*, *Science* **282**, 919 (1998).
24. We gratefully acknowledge the support of the NSF under CAREER award CHE-9733218. B.J.S. is a Cottrell Scholar of Research Corporation, an Alfred P. Sloan Foundation Research Fellow, and a Camille Dreyfus Teacher-Scholar.

13 April 2001; accepted 7 June 2001

## Impact of Polymer Tether Length on Multiple Ligand-Receptor Bond Formation

Claus Jeppesen,<sup>1</sup> Joyce Y. Wong,<sup>3</sup> Tonya L. Kuhl,<sup>4</sup> Jacob N. Israelachvili,<sup>1,2</sup> Nasreen Mullah,<sup>5</sup> Samuel Zalipsky,<sup>5</sup> Carlos M. Marques<sup>6\*</sup>

The promoters of cell adhesion are ligands, which are often attached to flexible tethers that bind to surface receptors on adjacent cells. Using a combination of Monte Carlo simulations, diffusion reaction theory, and direct experiments (surface force measurements) of the biotin-streptavidin system, we have quantified polymer chain dynamics and the kinetics and spatial range of tethered ligand-receptor binding. The results show that the efficiency of strong binding does not depend solely on the molecular architecture or binding energy of the receptor-ligand pair, nor on the equilibrium configuration of the polymer tether, but rather on its "rare" extended conformations.

How is the molecular structure and range of interaction of a given tethered receptor-ligand pair related to the interaction range and time required for binding? Our ability to answer this question is crucial to our understanding of biorecognition and bioadhesion. To investigate the impact of tether length and dynamics in modulating receptor-ligand binding, we chose a poly(ethylene glycol) (PEG) tether and the well-characterized ligand-receptor pair streptavidin-biotin (1–5). In the experi-

mental setup, shown schematically in Fig. 1, the biotin moiety is attached to the distal end of a flexible PEG tether while the streptavidin group is immobilized on the opposing membrane surface (6). Figure 2A shows the measured interaction forces between the two surfaces at varying separation distances for three tether lengths, expressed in terms of the polymerization index  $N$  (the number of  $CH_2CH_2O$  units) = 45, 75, and 142 (7).

The ligand-receptor binding range increases

REPORTS

with  $N$ . However, the measured binding or "capture" distances  $d_B$  (shown by the three vertical arrows in Fig. 2A as functions of  $N$ ) do not correspond to the calculated equilibrium average end positions  $R_e$  of the tethers. The

average end position of a polymer grafted to a wall at low densities is proportional to the Flory radius  $R_F$ , the average coil dimension in solution. If the solution is a good solvent for the polymer, the Flory radius scales as  $R_F = aN^{0.6}$ , where  $a$  is the size of an ethylene glycol monomer. The locus of  $R_e$ , obtained from the simulations presented below ( $\sim R_F$ ), is shown by the leftmost curve in Fig. 2B and falls well short of the measured binding distances  $d_B$  of Fig. 2A. As a further comparison, the rightmost curve in Fig. 2B shows the maximum possible binding distance, defined by the fully extended lengths of the PEG tethers,  $L = aN$ . Theoretically, this configuration has a zero chance of occurring over any finite time period. The measured binding curve for  $d_B$  falls between these two differ-

ent theoretical limits, defined by  $d_{avg} = R_e$  and  $d_{max} = L$ . The important question is: Given the typical tether lengths and reaction or collision time scales of biological interactions, what factors determine whether binding (capture) will or will not occur, and can this be predicted quantitatively?

Using a combination of Monte Carlo simulation and diffusion reaction theory, we demonstrate that the measured interaction forces are well explained in terms of the rare events when, over the experimental time scale, tethered molecules extend well beyond their average equilibrium configuration  $R_e$  across the gap; this extension enables a sufficient number of biotin ligands to bind to the opposing streptavidin pockets and pull the two surfaces together. Theoretically, the binding of a generic tethered ligand-receptor pair is expected to be governed by three main factors: (i) the intrinsic binding energy  $E_0$  of the ligand-receptor bond, (ii) the size and molecular structure of the terminal ligand moiety, and (iii) the length and molecular structure (which determines the flexibility) of the tether. For the class of tethered ligand-receptor pairs studied here,  $E_0$  is very large (several tens of  $k_B T$ , where  $k_B$  is the Boltzmann constant and  $T$  is absolute temperature), so that irreversible binding can be expected to occur once the ligand is within a few angstroms of the receptor ( $1-4$ ). Compared to the polymer tether, the biotin group is quite small, and it therefore has a much higher intrinsic translational and rotational mobility than the tether. As a consequence of these three

<sup>1</sup>Materials Research Laboratory, <sup>2</sup>Department of Chemical Engineering, University of California, Santa Barbara, CA 93106, USA. <sup>3</sup>Department of Biomedical Engineering, Boston University, 44 Cummington Street, Boston, MA 02215, USA. <sup>4</sup>Department of Chemical Engineering and Materials Science, University of California, 1 Shields Avenue, Davis, CA 95616, USA. <sup>5</sup>ALZA Corporation, 1900 Charleston Road, Mountain View, CA 94043, USA. <sup>6</sup>LDFC-Institut de Physique, 3 rue de l'Université, 67084 Strasbourg Cedex, France.

\*To whom correspondence should be addressed.

**Fig. 1.** Schematic illustration of the PEG-biotin and streptavidin molecular configurations used in the SFA experiments (3-5). Both membranes were in the solid phase so as to minimize lateral mobility. The PEG-biotin coverage was 4.5 mol %, giving a density  $\sigma$  of  $1.05 \times 10^{17} \text{ m}^{-2}$ , which corresponds to  $950 \text{ \AA}^2$  for each tethered ligand molecule. Each tether is composed of  $N$  ethylene oxide  $[-\text{CH}_2\text{CH}_2\text{O}-]$  monomer units of size  $a = 3.5 \text{ \AA}$ , where  $R_e$  is the corresponding average position of the PEG tether end obtained from the simulations, given by  $R_e \sim aN^{0.64} \approx R_F$  (Flory radius).  $R \approx 1 \text{ cm}$  is the (cylindrical) radius of curvature of each surface, and  $d$  is the distance from the outer edge of the streptavidin layer (of thickness  $45 \text{ \AA}$ ) to the lipid head group surface on the opposing membrane.

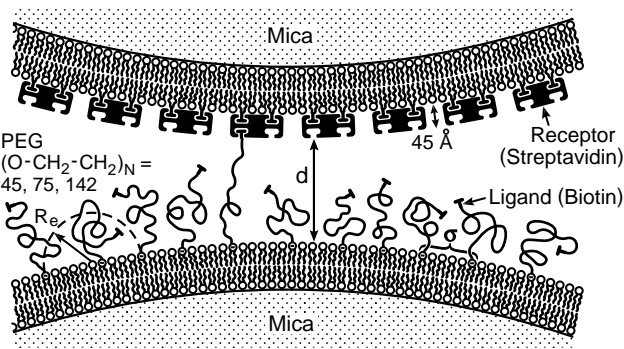
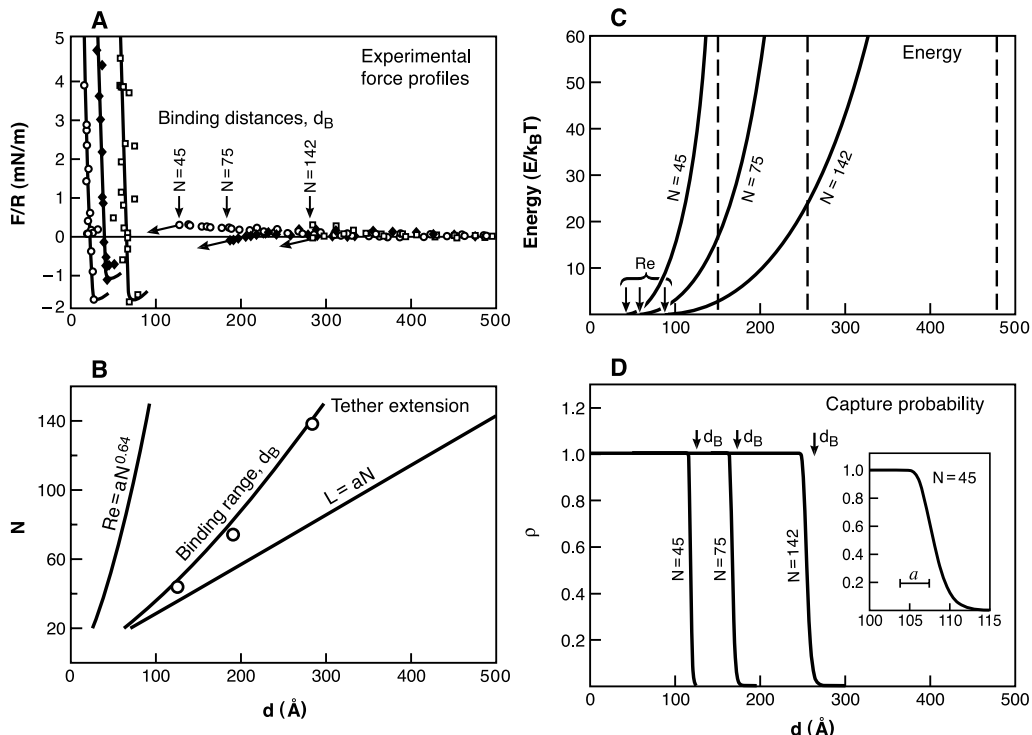


**Fig. 2.** Various measured and computed properties of the tethered ligand-receptor system as a function of distance  $d$ . (A) Normalized experimental force-distance curves ( $F/R$  versus  $d$ ) for the three tether lengths  $N = 45$  (circles),  $75$  (filled diamonds), and  $142$  (squares). The arrows indicate the points  $d_B$  at which the two surfaces spontaneously "jump" into adhesive contact, which occurs when sufficient biotin groups have bound to the opposing streptavidin receptors and the attractive "bridging" force exceeds the restoring force of the force-measuring spring. (B) Theoretical minimum and maximum binding distances defined by  $R_e$  and  $L$ . The experimentally measured binding or "capture" distances  $d_B$  (circles) and the Monte Carlo results (solid curve), computed for a "reaction" or "collision" time of  $\tau = 1 \text{ s}$ , agree with each other and fall between the two limiting theoretical curves. (C) The extension energy curves from the Monte Carlo simulations described in the text. In the limit of strongly stretched, short chains ( $N < 100$ ), the energy of the polymer tether can be approximated by  $E = Nk_B T \log[2.15(1 - d/L)]$ . (D) Capture probability after the opposing surfaces have been exposed for  $1 \text{ s}$  at a distance  $d_B$ , as a function of the polymerization index  $N$ . The values for  $d_B$  appear as the solid middle curve in Fig. 2B. A comparison of  $d_B \approx 110 \text{ \AA}$  to the monomer length  $a = 3.5 \text{ \AA}$  is shown in the inset for  $N = 45$  (where  $L = aN \approx 150 \text{ \AA}$ ).



factors, the binding mechanism of this system is expected to be controlled mainly by the dynamics of the polymer tether (i.e., by the energetics associated with extended polymer configurations).

Several theoretical approaches have been proposed to describe the extended configurations of flexible polymer tethers in terms of their extensional energies  $E(d)$  and associated forces  $f(d) = -\partial E/\partial d$ , where  $d$  is the separation between the two ends. However, no theory currently accounts for the combined effects of finite extensibility of the chain, monomer excluded volume, and the impenetrability of the two confining walls. We have analyzed this system with Monte Carlo simulations (8). First, for each  $N$ , a force-distance plot  $f(d)$  was generated (9, 10). Integrating the  $f(d)$  curve (11) yields the energy

$$E(d) = \int_{R_c}^d f(h)dh \quad (1)$$

(Fig. 2C), where  $h$  is the force to stretch a polymer chain. The curves diverge [ $E(d) \rightarrow \infty$ ] at complete extension of the chains ( $d \rightarrow L$ ), shown by the three vertical dashed lines in Fig. 2C. The equilibrium (minimum energy, zero force) position of the ends occurs at  $R_c = N^{0.64}a$ , where the exponent of 0.64 is close to the Flory exponent  $\nu = 0.59$  for the average dimension of asymptotically large polymer chains in a good solvent (12). These equilibrium energy-distance curves, however, do not give the binding distances  $d_B$ ; to obtain these distances, we must also include the reaction or collision time  $\tau$  in the analysis. At the most probable end position  $d = R_c$ , a given chain population will bind very fast, on the order of the chain relaxation time ( $10^{-8}$  to  $10^{-5}$  s). At  $d = L$ , binding will eventually occur, but only after an exceedingly long “waiting” time. The question then becomes: At what separation  $d$  will binding occur when the waiting time is about 1 ms (a typical biological collision time) or 1 s (the experimental waiting time)?

When complementary binding groups on two approaching surfaces are brought to within a distance  $d$  of each other that is slightly smaller than the fully extended tether length  $L$ , a spontaneous binding reaction can occur, but the probability of this is low. This probability depends on the time the surfaces are kept at this separation, or (for multiple interactions) on the number of tethered ligands involved in the interaction. This is directly proportional to the product of the coverage density  $\sigma$  and the area of the interacting surfaces. At any given separation  $d < L$ , there will be a progressive buildup of the net attractive force  $F(d,t)$  between the two surfaces as more and more bridges form with time  $t$  (assuming irreversible binding). This force is given by summing the number of bound chains at time  $t$ , which can be derived

in terms of the probability that a reaction or binding event occurs at time  $t$  after the surfaces are brought to the separation distance  $d$ . The experimentally measured force between two surfaces in the surface forces apparatus (SFA) experiments is then given by

$$F(d,t) = 2\pi R\sigma \int_d^\infty \rho(h,t)f(h)dh \quad (2)$$

(13), where  $\rho(h,t)$  is the fraction of chains bound,  $f(h)$  is the force contribution from each individual chain (14), and the other parameters are defined as in Fig. 1.

Determination of the parameter  $\rho(d,t)$  can be obtained from the diffusion-reaction theory for polymers (15–19). If we take the ligand-receptor binding reaction at  $d$  to occur at a fast frequency  $q$ , the bound fraction  $\rho(d,t)$  can be shown (16–18, 20) to be a single-exponential function given by

$$\rho(d,t) = 1 - e^{-t/\tau(d)} \quad (3)$$

where the decay time  $\tau(d)$  is independent of  $q$ . Thus, at  $t = 0$ ,  $\rho(d,0) = 0$  and no chains are bound, whereas at  $t = \infty$ ,  $\rho(d,\infty) = 1$  and all chains are bound. For weaker ligand-receptor pairs,  $\tau(d)$  is likely to depend on the binding frequency  $q$  according to  $\tau(d) \approx 1/q$  (21).

Using our result for  $\tau(d)$  and the relaxation function  $j(t)$  for a Zimm chain (19), we can draw a direct comparison between the experimental results and theoretical predictions. At a separation distance  $d$ , the fraction  $\rho$  of chains that have reacted during the experimental time  $t_{\text{exp}}$  is given by Eq. 3 as

$$\rho(d,t_{\text{exp}}) = 1 - e^{-t_{\text{exp}}/\tau(d)} \quad (4)$$

Figure 2D shows the calculated fraction  $\rho(d,t_{\text{exp}})$  at  $t_{\text{exp}} = 1$  s for  $N = 45, 75$ , and 142 (22). In the calculation we used the potential energy obtained from the Monte Carlo simulations for each value of  $N$  (see Fig. 2C). As shown in Fig. 2D, the function  $\rho(d,t_{\text{exp}} = 1 \text{ s})$  changes fairly abruptly from zero to unity at distances  $d_B$  that lie between  $R_c$  and  $L$  as determined by  $t_{\text{exp}}$ . Moreover, the calculated values for  $d_B$  quantitatively account for the observed abrupt onsets of the attractive forces measured in the SFA experiments at  $d = 125 \pm 5 \text{ \AA}$ ,  $190 \pm 14 \text{ \AA}$ , and  $284 \pm 20 \text{ \AA}$ , for the three tether lengths  $N = 45, 75$ , and 142, respectively (Fig. 2A). A comparison of the calculated extension to the experimental results is also shown by the middle curve for  $d_B$  in Fig. 2B. Note that the relative elongation ( $d_B/L$ ) at which binding occurs decreases with increasing  $N$ .

The above analysis explains, both qualitatively and quantitatively, the effect of flexible tethers on the kinetics and spatial range of multiple ligand-receptor binding. First, the tether acts to extend the spatial sampling of the ligands, enabling them to bind to receptor pockets at distances approaching the full tether length  $L$  as  $t \rightarrow \infty$ . Second, in the case of small ligands, the dynamics of the spatial exploration

of the ligand is not simply that of a diffusing particle but is governed or biased by the dynamics of the tether chain. Third, the specific ligand-receptor binding energy  $E_0$  acts to tune how much of the total energy landscape  $E(d,t)$  needs to be explored by the tether before binding occurs, thus setting the back-reaction rate or likelihood of bond dissociation (1). Thus, a combination of the specific ligand-receptor pair interaction and the dynamics of the tethering chains determines the overall range, rate, and ultimate strength of complementary multiple bond formation.

These results suggest that “tethered binding kinetics” should be considered in detail, and as a process, when describing dynamic bond formation (and dissociation), where the intrinsic binding energy  $E_0$  of the adhering molecules is just one of many factors that determine the time evolution of a binding event.

#### References and Notes

1. N. M. Green, *Adv. Protein Chem.* **29**, 85 (1975).
2. E. L. Florin, V. T. Moy, H. E. Gaub, *Science* **264**, 415 (1994).
3. D. E. Leckband *et al.*, *Biochemistry* **33**, 4611 (1994).
4. C. A. Helm *et al.*, *Proc. Natl. Acad. Sci. U.S.A.* **88**, 8169 (1991).
5. J. Y. Wong *et al.*, *Science* **275**, 820 (1997).
6. Both the streptavidin and PEG-biotin membrane surfaces are constructed using Langmuir-Blodgett deposition of phospholipid bilayers and self-assembly from solution onto molecularly smooth mica substrates.
7. Polydispersities of our samples range from 1.001 to 1.004, as determined by matrix-assisted laser desorption/ionization (MALDI) mass spectrometry.
8. The Monte Carlo simulations were based on a “pearl necklace” model for a polymer chain end grafted to two impenetrable parallel surfaces. In our simulations, one surface was kept fixed and the other was allowed to move vertically under the control of a force  $F$ . Histograms were generated for each chain length to yield the force versus polymer extension.
9. A. M. Ferrenberg, R. H. Swendsen, *Phys. Rev. Lett.* **61**, 2635 (1988).
10. ———, *Phys. Rev. Lett.* **63**, 1195 (1989).
11. To ensure an error less than 1%, we used 14 different values of the force from  $f = 0$  to  $f_{\text{max}}$  (90% extension) so that histograms would overlap significantly from one value of the force to the next. For each value of the force and  $N$ , we generated  $6.6 \times 10^8$  configurations and sampled  $3.0 \times 10^5$  of those.
12. P. G. deGennes, *Scaling Concepts in Polymer Physics* (Cornell Univ. Press, Ithaca, NY, 1979).
13. J. N. Israelachvili, *Intermolecular & Surface Forces* (Academic Press, London, ed. 2, 1992).
14. Computing the total force as the sum of individual chain contributions is certainly accurate in our case, where the average equilibrium configurations of the anchored tethers barely overlap on each surface (namely,  $\sigma \sim R_c^2$  in Fig. 1). However, this would be a poor approximation for describing higher anchoring densities or compressions, where excluded volume interactions between chains play a dominant role.
15. H. A. Kramers, *Physica (Utrecht)* **7**, 284 (1940).
16. G. Wilemski, M. J. Fixman, *Chem. Phys.* **58**, 4009 (1973).
17. M. Doi, *Chem. Phys.* **9**, 455 (1975).
18. P. G. deGennes, *J. Chem. Phys.* **76**, 3316 (1982).
19. We start from the integral form of the generalized reaction-diffusion equation for the probability density associated with the tether end:

$$\psi(r;t) = \psi_{\text{eq}}(r) - \int dt \int dr_0 G(r,r_0;t) \psi(r_0;t) Q(r_0)$$

where  $\psi_{\text{eq}}(r)$  is the equilibrium distribution of end-to-end vectors in the absence of reactions (binding

# Physical Structure and Inversion Charge at a Semiconductor Interface with a Crystalline Oxide

R. A. McKee, F. J. Walker, M. F. Chisholm

We show that the physical and electrical structure and hence the inversion charge for crystalline oxides on semiconductors can be understood and systematically manipulated at the atomic level. Heterojunction band offset and alignment are adjusted by atomic-level structural and chemical changes, resulting in the demonstration of an electrical interface between a polar oxide and a semiconductor free of interface charge. In a broader sense, we take the metal oxide semiconductor device to a new and prominent position in the solid-state electronics timeline. It can now be extensively developed using an entirely new physical system: the crystalline oxides–on–semiconductors interface.

Inversion charge associated with field-effect phenomena at oxide/semiconductor interfaces can be described using Maxwell's first equation  $\nabla \cdot \mathbf{D} = \rho$ , where  $\mathbf{D}$  is the dielectric displacement in the oxide and  $\rho$  is the inversion charge in the semiconductor. Our understanding of the electrostatics of field-effect phenomena deduced from this expression relies on the assumption that dielectric displacement is continuous at the oxide/semiconductor interface. This assumption, with its application in SiO<sub>2</sub>/Si capacitors (1), is the foundation of essentially all of modern metal oxide semiconductor (MOS) device physics. Because alternative materials are being considered as replacements for the amorphous SiO<sub>2</sub> dielectric on silicon, however, and particularly because attempts to add higher functionality to a silicon platform are being made, we would do well to reconsider how physical structure at oxide/semiconductor interfaces couples to inversion charge.

Much of the effort expended to date in the search for an alternative to SiO<sub>2</sub> has focused on amorphous oxides, attempting to extend the SiO<sub>2</sub>/Si concept. Although this approach is attractive, defects at an amorphous/crystalline interface associated with steric hindrance and bond coordination (2, 3) can lead to a discontinuity in dielectric displacement. Maintaining continuity in dielectric displacement via passivation of these defects with hydrogen is a convenience that works for SiO<sub>2</sub>/Si, but it is a methodology that is not universally applicable. Steric hindrance and the statistical nature of defect formation with directional bonding are intrinsic to an amorphous/crystalline boundary, but these defects can be avoided entirely with a crystalline structure at a polar oxide/semiconductor interface (4).

Here we consider crystalline oxides on semiconductors (COS) as candidate solutions to the alternative gate dielectrics problem and suggest their much broader potential for new function-

ality in solid-state electronics. Our thesis is that the physical structure at a COS interface can be made perfectly commensurate, and that in such a state, the systematics of crystalline periodicity lead to an unprecedented ability to manipulate dielectric displacement and inversion charge at a dielectric/semiconductor surface. This notion thus has implications for entirely new device physics and a device functionality that cannot even be considered with SiO<sub>2</sub> on silicon.

Looking at the physical structure of COS, a three-panel construction of Z-contrast images is shown (Fig. 1) of Ba<sub>0.725</sub>Sr<sub>0.275</sub>O and SrTiO<sub>3</sub> on pure silicon and of BaTiO<sub>3</sub> on pure germanium, all grown using molecular beam epitaxy (MBE) techniques. The Ba-Sr-O compound (Fig. 1A) has a 5-eV band gap (5) and is alloyed to match the lattice parameter of the (001) face of silicon. The overlay in the left side of the image shows a simple model of the epitaxial cube-on-cube NaCl-type oxide structure of the alkaline earth oxide on silicon. Although the oxygen atoms are not imaged, the bright contrast of the heavy alkaline earth metal atoms and the [110] symmetry of the epitaxial structure are clear. The case in which SrTiO<sub>3</sub> has been grown and strained 2% to be commensurate to silicon is illustrated in Fig. 1B, and BaTiO<sub>3</sub> on germanium with its room-temperature lattice match is shown in Fig. 1C.

These lattice images are members of a COS structure series that can be generically written as (AO)<sub>n</sub>(A'BO<sub>3</sub>)<sub>m</sub>. The subscripts *n* and *m* in this structure series are integer repeats of atomic planes and unit cells of constituent crystalline layers. Although this structure series can be quite broadly applied, we will discuss it here for cases where A and A' are elements or combination of elements out of group IIA of the periodic table (that is, Ba, Sr, Ca, and Mg) and B is a group IVA transition metal such as Ti or Zr.

In analogy to III-V gallium arsenide alloy heteroepitaxy (6), our oxide MBE synthesis technique (4, 7, 8) has shown that lattice-matched oxides can be formed in our struc-

events), and *G* is the dynamic propagator of the end-vector distribution. The sink operator *Q* draws the reacted biotin ends at a rate

$$d(1 - \rho)/dt = - \int \psi(r;t)Q(r)dr$$

from the probability distribution. The form  $Q(r) = q\delta(z - d)$  (where  $\delta$  is the delta function) is ascribed to the sink operator, which removes the bound biotin chains at a distance *d* with frequency *q* from the total population. The *q*-independent decay rate of the exponential long-time behavior,  $t(d)^{-1}$ , is given by

$$\tau(d) = \exp[E(d)] \int_0^\infty dt \left\{ \frac{1}{\sqrt{1-j(t)^2}} \exp \left[ -E(d) \frac{1-j(t)}{1+j(t)} \right] - \exp[-E(d)] \right\}$$

where *E*(*d*) is the value of the potential (now in *k<sub>B</sub>T* units) at position *d*, and *j*(*t*) is a model-dependent relaxation function for the end-to-end distance of the polymer tether. This result generalizes Kramers' expression for the escape time over a potential barrier (75) by accounting for internal chain dynamics. The main weighting factor grows exponentially with the height of the barrier, and the dynamics close to the reaction point (*d<sub>0</sub>*) determine how fast the terminal escape path is performed. For a harmonic oscillator,

$$j(t) = \exp(-t/\tau_0) \sim 1 - t/\tau_0$$

and our result reduces to Kramers' for the escaping time of a particle over a harmonic potential that ends at distance *d*. For the Rouse chain, the collective short-time behavior is nondiffusive, yielding

$$j(t) \sim 1 - 4/\pi^{3/2}(t/\tau_r)^{1/2}$$

leading to

$$\tau(d) = \tau_r \pi^{7/2}/8 \exp[E(d)]/E(d)^{3/2}$$

Thus, the terminal exploration time is a factor *E*(*d*) faster for the Rouse chain, which demonstrates the influence of internal tether dynamics on the binding event. Likewise, the Zimm relaxation function

$$j(t) \sim 1 - 1.3(t/\tau_z)^{2/3}$$

of a polymer chain in a good solvent takes hydrodynamics into account, and the reaction time is then

$$\tau(d) = [1.43\tau_z/E(d)] \exp[E(d)]$$

20. A. Kolb, C. M. Marques, G. H. Fredrickson, *Macromol. Theory Simul.* **6**, 169 (1997).

21. D. J. Bicout, A. Szabo, *J. Phys. Chem.* **106**, 10292 (1997).

22. The time scale of 1 s is based on our SFA experiments, where the opposing surfaces approach each other at a rate of 1 Å/s. Strictly speaking, for an experiment performed under some approaching speed *v*(*t*), the gap thickness *d* is a function of time

$$d(t, v) = d_0 - \int_0^t v(t') dt'$$

and the binding kinetics is also a function of the velocity *v*(*t*). For low speeds, the bound fraction is approximately given by

$$\rho = 1 - \exp\left(-\int_0^t dt' / \tau[d(t'), v(t')]\right)$$

However, the binding time is a very steep function of the distance *d* and, for all practical purposes, the typical binding distance can be evaluated by simply setting  $t_{\text{exp}} = \tau(d)$ .

23. We thank P. Bongrand and F. Pincus for fruitful discussions. Supported by NIH grants GM-47334 and GM-17876, UCSB Materials Research Laboratory grant DMR 96-32716, U.S. Department of Energy Presidential Early Career Award for Scientists and Engineers award 05419-0099-2K, the Chemistry Department of the CNRS under Actions Incitatives sur Programme "Soutien aux Jeunes Equipes," and the Henry Luce Foundation (Clare Boothe Luce Professorship).

26 February 2001; accepted 8 June 2001 Physical

Oak Ridge National Laboratory, Oak Ridge, TN 37831-6118, USA.